Journal of Materials Chemistry A

PAPER

Cite this: J. Mater. Chem. A, 2018, 6, 17706

Evaluation of the highly stable metal–organic framework MIL-53(Al)-TDC (TDC = 2,5-thiophenedicarboxylate) as a new and promising adsorbent for heat transformation applications†

Niels Tannert, ‡[a] Sebastian-Johannes Ernst, ‡[bc] Christian Jansen, [a] Hans-Jörg Bart, [b] Stefan K. Henninger[c] and Christoph Janiak *[a]

Received 11th May 2018
Accepted 22nd August 2018

DOI: 10.1039/c8ta04407d

rsc.li/materials-a

The recently reported Al-based metal–organic framework MIL-53(Al)-TDC (TDC = 2,5-thiophenedicarboxylate) shows desirable water sorption properties towards adsorption-driven heat transformation applications with high thermal and solvent/pH stability as well as hydrothermal stability over 40 cycles. Water vapor sorption measurements at 25, 40 and 60 °C yielded an advantageous isosteric heat of adsorption of only 2.6 kJ g^{-1}, favoring the use of MIL-53(Al)-TDC in sorption based chilling where the released heat of adsorption corresponds to waste heat. The good cooling performance of MIL-53(Al)-TDC comes from desirable low desorption temperatures below 65 °C, with also desirable high condenser temperatures of around 40 °C and corresponding water exchange of almost 0.35 g g^{-1}. The thereby offered working window cannot be provided by common adsorbents and renders the material an ideal candidate for adsorption cooling applications.

Introduction

Metal–organic frameworks (MOFs) receive continuous attention due to their unsurpassed porosity and chemical variability, which originate from the inherent modular cluster–linker concept.[1] The organic linkers in MOFs are typically bi-, tri- or tetradentate carboxylates.[2] Linker modulation enables tailoring of the properties of a MOF towards applications[3,4] and has yielded thousands of MOFs with a broad range of properties to date.[5,6]

Of recent interest is the application of MOFs in the field of water sorption/harvesting[7,8] and related sorption heat transformation processes.[9–11] Fig. 1 illustrates the underlying principle of heat transformation that can be separated into two stages: a working cycle and a regeneration cycle. During the working cycle, a working fluid is evaporated taking up ambient heat for the evaporation (Q_{evap}), while the adsorbent adsorbs the working fluid, releasing the heat of adsorption (Q_{ads}). As soon as the adsorbent is sufficiently loaded, the regeneration cycle is started by applying heat to the adsorbent (Q_{des}). The desorbed working fluid is condensed releasing heat of condensation (Q_{cond}).

Typically, two types of applications arise from this principle: adsorption heat pumps and adsorption chillers. In heat pumps, the released Q_{ads} and Q_{cond} provide a heating system at a medium temperature level, *e.g.* floor heating at 40 °C, whereas Q_{evap} comes from the environment at typically 10 °C. In the chilling mode, Q_{evap} is the amount of heat that can be used to

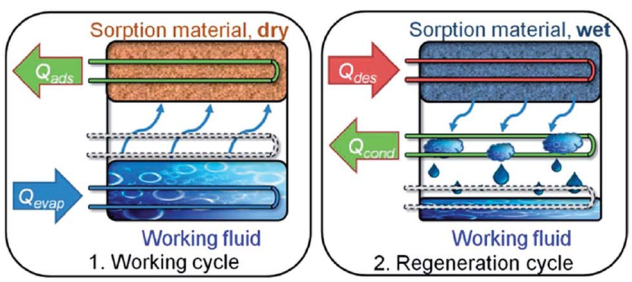

Fig. 1 In the working cycle, a working fluid (favorably water due to its high evaporation enthalpy and no toxicity) is evaporated, taking up evaporation heat Q_{evap}. During incorporation into a porous material, adsorption heat Q_{ads} is released. In the regeneration cycle, driving heat Q_{des} for desorption is applied, and further condensation takes place at a medium temperature level and releases condensation heat Q_{cond}. The device can be used as a chiller or a heat pump. The image was taken with permission from ref. 13.

[a]Institut für Anorganische Chemie und Strukturchemie, Heinrich-Heine-Universität Düsseldorf, 40204 Düsseldorf, Germany. E-mail: janiak@uni-duesseldorf.de

[b]Chair of Separation Science and Technology, TU Kaiserslautern, Postfach 3049, 67653 Kaiserslautern, Germany

[c]Fraunhofer Institute for Solar Energy Systems (ISE), Heidenhofstr. 2, 79110 Freiburg, Germany

† Electronic supplementary information (ESI) available: Synthesis details, further (*in situ*) PXRD and TGA, nitrogen (77 K), argon (87 K) and water (20 °C) sorption isotherms, multicycle stability tests, SEM images and more information on methods and devices. See DOI: 10.1039/c8ta04407d

‡ These authors contributed equally.

chill, *e.g.*, an industrial process, whereas Q_{ads} and Q_{cond} can be considered waste heat, which is dissipated to the environment. In both cases, Q_{des} is the amount of heat that has to be provided to drive the process. Desorption temperatures below 100 °C are mostly favored, since they can easily be reached by solar thermal heat or industrial waste heat. Utilization of the energies Q_{evap} or Q_{ads} and Q_{cond} occurs by continuous cycling of the adsorbent.[12,13]

Sorption heat transformation is gaining more and more attention, as the proof of concept has already been demonstrated on a pre-industrial scale.[14–16] Thermally driven heat transformation is a promising approach towards energy efficient heating and cooling,[17] since both the efficiency and cost effectiveness of such processes are critically governed by the performance of the applied adsorbents. Therefore, many MOFs have been investigated with respect to application in thermally driven heat transformation, looking mainly at water sorption and stability characteristics.[18–22]

Since MOFs can show a significant loss of retention of surface area and crystallinity after water sorption,[23] hydrothermal cycle stability is one key factor for utilization of MOF materials in such applications.[9,13,24–26]

There is a rising demand for adsorbents with tailor-made water sorption properties,[27,28] which is underlined by the ongoing research towards both new materials[15,29–31] and pre-industrial scale applications.[9,12,16]

An important performance indicator for the evaluation of porous materials in heat transformation applications is the working fluid uptake capacity together with adsorption and desorption within the possible temperature boundaries for heat of evaporation (Q_{evap}), driving heat (Q_{des}) and heat dissipation or useful heat in the heat pumping mode (Q_{ads} and Q_{cond}). For cooling applications the material must be capable of evaporating the working fluid from as low as possible reservoir temperatures and still showing an uptake when itself reaches as high as possible temperatures through Q_{ads}. The latter is more effectively dissipated to the environment from an as high as possible temperature level. For regeneration, an as low as possible temperature level for Q_{des} is desirable together with an as high as possible temperature level for the dissipation of Q_{cond}.

In particular Al-based MOFs proved to be highly thermally and hydrolytically stable and therefore most suitable for heat transformation applications,[9,13,26,32] and furthermore Al is an abundant, inexpensive light metal with low toxicity.

The most investigated Al-MOFs for sorption heat transformation are MIL-100 (linker = trimesate, MIL = Matériaux de l'Institut Lavoisier),[13,33,34] Al-fumarate (linker = fumarate, trade name Basolite A520),[35] CAU-10 (linker = isophthalate, CAU = Christian-Albrechts-Universität)[36] and MIL-160 (linker = 2,5-furandicarboxylate).[18] These Al-MOFs exhibit pore sizes in the microporous region, yielding pore filling with water vapor at relative pressures around $0.1 < p/p_0 < 0.4$, which is an ideal range for sorption heating and cooling.[10,37,38]

In 2017 Maurin and co-workers presented theoretical calculations for promising water sorption properties of ligand functionalized MIL-160 materials, including the linker 2,5-thiophenedicarboxylate (TDC) (Fig. 2).[39] In this case, they predicted an isotherm with an inflection point of $\alpha = 0.19$ and an uptake of 0.44 g g^{-1}. Recently, Stock *et al.* published a new Al-based MOF with the MIL-53 topology (Fig. 2).[40] It was denoted as MIL-53(Al)-TDC and proven to exhibit 0.469 g g^{-1} water uptake at $\alpha = 0.19$, displaying the formula [Al(μ-OH)(TDC)] and comprising lozenge-shaped pores with a diameter of 8 × 8.2 Å.

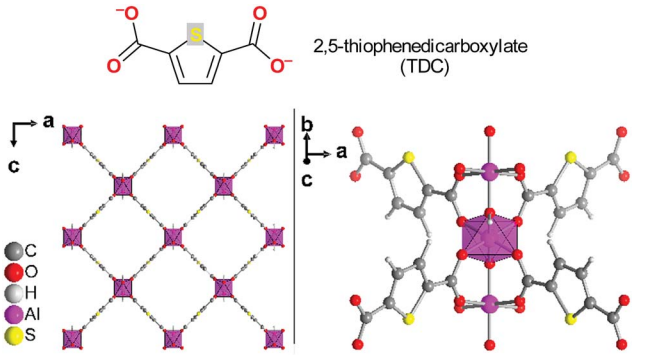

Fig. 2 (Top) The linker 2,5-thiophenedicarboxylate (TDC). (Bottom, left) Section of the packing diagram of MIL-53(Al)-TDC viewed along the channels with a cross-section of approximately 8 × 8.2 Å. (Bottom, right) Extended secondary building unit (SBU) with *trans* corner-sharing AlO_6 octahedra. The graphics were produced from a cif-file that was generously provided by Serre and co-workers.

MIL-53(Al)-TDC was found to exhibit porosity parameters of BET = 1150 m^2 g^{-1} (BET = Brunauer–Emmett–Teller), a micropore volume of 0.48 cm^3 g^{-1} and a maximum water vapor uptake of 469 mg g^{-1}.[40] Parallel to our study, MIL-53(Al)-TDC was evaluated for CO_2 capture.[41] Stock and co-workers suggested its applicability in the field of heat transformation processes due to the desirable S-shape of the water isotherm, relatively high water uptake in a good pressure region, and high thermal stability.[40] Herein we thoroughly characterize MIL-53(Al)-TDC towards cyclic water sorption heat transformation applications.

Experimental

Materials and instrumentation

All chemicals were used as received from suppliers. For further information about all materials see Section S1 in the ESI.†

Powder X-ray diffractometry (PXRD) was performed at ambient temperature on a D2 phaser (Bruker, Billerica, US) using Cu-K$_\alpha$ radiation ($\lambda = 1.54182$ Å) in the range of $5° < 2\Theta < 50°$ with a scan rate of 0.0125° s^{-1} (300 W, 30 kV, 10 mA). Analyses of the diffractograms were carried out with Match 3.11 software.

Thermogravimetric analysis (TGA) was carried out on a Netzsch TG209 F3 Tarsus (Netzsch, Selb, Germany) device under a nitrogen atmosphere and heating at a ramp rate of 5 K min^{-1} to the target temperature (600 °C).

Elemental analysis was performed on a vario MICRO cube (Elementar Analysensysteme, Langenselbold, Germany).

Infrared spectra were acquired on a Bruker Tensor 37 FT-IR device. SEM images were acquired on a JEOL JSM-6510

advanced electron microscope (Jeol, Akishima, Japan) with a LaB_6 cathode at 5–20 keV. The microscope was equipped with an Xflash 410 (Bruker, Billerica, US) silicon drift detector.

Surface areas (BET) were determined by nitrogen (purity 99.999%, 5.0) sorption experiments at 77 K using liquid nitrogen with a Quantachrome NOVA-4000e (Quantachrome, Odelzhausen, Germany) instrument within a partial pressure range of $p/p_0 = 10^{-3}$ to 1 bar. Each sample was degassed under vacuum (<10^{-2} mbar) at 150 °C for *ca.* 3 h, prior to measurement. All surface areas (BET) were calculated from five adsorption points in the pressure range p/p_0 = 0.005–0.05 by applying Roquerol plots (r > 0.998). This range is indeed not recommended by IUPAC (International Union of Pure and Applied Chemistry) for BET surface area determination, but is also suitable for microporous materials.[42] Total pore volumes were calculated from the N_2 sorption isotherm at p/p_0 = 0.95. NLDFT calculations for the pore size distribution curves were performed with the native NovaWin 11.03 software using the 'N_2 at 77 K on carbon, slit pore, NLDFT equilibrium' model. Argon (purity 99.999%, 5.0) sorption experiments were done at 87 K using a Quantachrome cryocooler (Quantachrome, Odelzhausen, Germany) for appropriate adjustment of T = 87 K on a Quantachrome Autosorb iQ MP (Quantachrome, Odelzhausen, Germany) instrument within a partial pressure range of $p/p_0 = 10^{-7}$ to 1 bar. All water sorption isotherms (25, 40, and 60 °C) were measured with a Quantachrome VStar4 (Quantachrome, Odelzhausen, Germany) within a partial pressure range of $p/p_0 = 10^{-3}$ to 0.9 bar.

Water cycling stabilities were examined with a Setaram™ TGA-DSC-111 (Setaram, Caluire, France) on powdered samples. A humidified argon gas flow (40 °C, 76.3% relative humidity) was generated by a Setaram™ WetSys (Setaram, Caluire, France) humidity controller and passed through the sample chamber, while the temperature of the sample was varied and the mass of the adsorbent was monitored. For the multi-cycle adsorption/desorption experiments, the temperature of the sample was varied between 40 °C and 140 °C with a cycle time of 5 h.

More detailed information on analytical procedures is given in the ESI.†

Reflux synthesis optimization

In order to find a reliable ambient pressure synthesis instead of the only reported solvothermal route for MIL-53(Al)-TDC, we performed synthesis optimization according to Tschense *et al.* in mixtures of water and dimethylformamide (DMF) (4 : 1).[40]

Generally, Al-MOFs are synthesized using various Al reagents and it remains somehow unclear what source of Al is advantageous for the formation of [Al(OH)(linker)]-type MOFs. Therefore, we developed a reflux synthesis (135 °C, 24 h) with varying Al sources (Table 1 and Section S2 in the ESI†) and obtained the desired product as a microcrystalline powder in each case. Formation of the desired phase already took place within a few hours; however, we carried out the reaction for 24 h to ensure the completeness of the reaction and superior porosity. Structural verification was performed by PXRD (Fig. S1†) and nitrogen sorption studies (Table 1 and Fig. S13 in the ESI†).

Table 1 Synthesis results of MIL-53(Al)-TDC with different starting materials

Al source	BET[a] [$m^2\ g^{-1}$]	Pore volume[b] [$cm^3\ g^{-1}$]	Yield [%]
$Al(OH)(ac)_2 \cdot xH_2O$	885, 1092	0.41, 0.52	95, 91
$NaAlO_2$	395	0.37	39
$Al_2(SO_4)_3 \cdot 18H_2O$	1102	0.46	88
$AlCl_3 \cdot 6H_2O$	1096	0.49	83
Ref. 40[c]	1150	0.48	84

[a] Determined by five adsorption points of nitrogen isotherms in the range 0.005 < p/p_0 < 0.05. [b] Determined using the NLDFT method (carbon, slit pore, nitrogen, 77 K) at p/p_0 = 0.9. [c] Micropore volume at p/p_0 = 0.5.

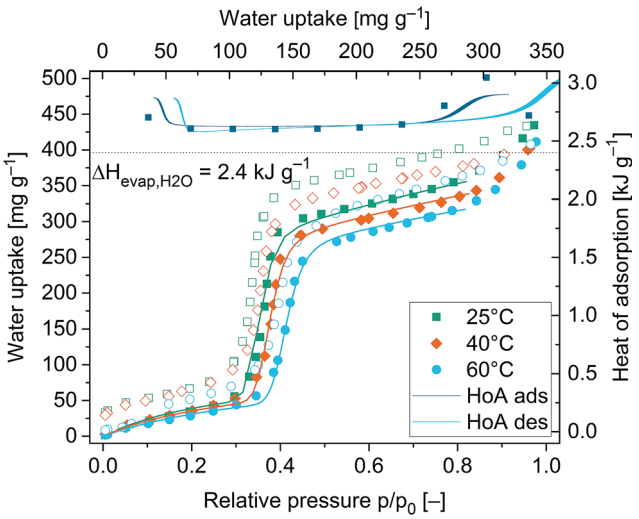

Fig. 3 Water sorption isotherms at three different temperatures (filled symbols: adsorption and open symbols: desorption) and differential heat of adsorption determined from the adsorption (dark blue line) and desorption (light blue line) branches of the isotherm. The solid lines in the adsorption isotherms symbolize simulations with a weighted dual site Langmuir (wDSL) approach (see Section S13, ESI†). The dotted line with $\Delta H_{evap,H_2O}$ = 2.4 kJ g^{-1} marks the heat of vaporization of water at 25 °C.

Results and discussion

Synthesis optimization

Within the described optimization towards a reflux-based synthesis we tested the following Al reagents: $AlCl_3$, Al(OH)(acetate)$_2$, $Al_2(SO_4)_3$ and $NaAlO_2$. All products were characterized by PXRD and nitrogen sorption. The PXRD patterns of all MIL-53(Al)-TDC compounds showed similar crystallinity, revealing the robustness of the formation of the MOF phase (Fig. S1 in the ESI†).

From scanning electron microscopy images the products were microcrystalline agglomerates (Fig. S8–S11 in the ESI†). Except for $NaAlO_2$ as the Al source, all obtained products were in the same range of crystallinity and porosity (Table 1 and Fig. 1, see also ESI†).

Besides the difference in porosity, the Al source shows influence on the water sorption performance, mostly in terms of

uptake, which in turn directly correlates with the pore volume (nitrogen sorption: Fig. S12† and water sorption: Fig. S14 in the ESI†). More information can be found in the ESI.†

Stability tests

Additionally, we performed solvent stability tests by dispersing *ca.* 10 mg of MIL-53(Al)-TDC into 3 mL of different solvents and stirring the dispersion for 24 h. By PXRD, no loss of crystallinity was apparent in any solvent. At least partial decomposition and loss of crystallinity occurred within 24 h in aqueous solutions with pH 12 and pH 1 (Fig. S3 and S4 in the ESI†).

Further characterization with infrared spectroscopy (IR), and thermogravimetric analysis (TGA), scanning electron microscopy (SEM), and argon (87 K), nitrogen (77 K) and water (20 °C) sorption isotherms of MIL-53(Al)-TDC products from synthesis optimization are provided in the ESI.†

All further analyses were carried out with the material synthesized from $Al(OH)(ac)_2$ (BET = 885 $m^2\ g^{-1}$ from nitrogen sorption, *i.e.* 827 $m^2\ g^{-1}$ from argon sorption, see Section S11 in the ESI†). This approach showed the highest yield and satisfactory porosity.

Water sorption characteristics

In order to evaluate the potential of MIL-53(Al)-TDC for thermally driven heat transformation, water sorption isotherms were measured at 25, 40 and 60 °C. Prior to the measurements, each sample was activated at 150 °C under reduced pressure. Fig. 3 shows the water adsorption isotherms, where the solid lines represent thermodynamic fits. The adsorption isotherms show an S-shaped type-V isotherm according to the IUPAC classification,[42] with a steep increase of the uptake at relative pressures in the range $0.35 < p/p_0 < 0.4$. This uptake is correlated with filling of the micropores. The maximum uptake is about 434 $mg_{H_2O}\ g^{-1}$. Such an adsorption characteristic is comparable to that of aluminium fumarate, but slightly less hydrophilic, allowing desorption at higher relative pressures, synonymous with lower desorption temperatures.

Furthermore, the isotherms show a slight hysteresis at all temperatures, especially for the uptake after the steep rise that has been attributed to kinetic inhibition.[40] However, hysteresis behaviour occurs on different scales. Yet, a water sorption hysteresis is undesired for the targeted application, because it decreases the usable range of the working fluid exchange within the cycle.[13] Only MIL-53(Al)-TDC obtained from aluminium sulfate and from basic aluminium acetate showed water desorption with almost absence of hysteresis (Fig. S14 in the ESI†). The absence of hysteresis is explained by a lower number of defects. Defects in the form of missing linkers and terminal Al–OH and $Al–OH_2$ groups will provide stronger binding sites and mesoporous cavities with kinetically delayed desorption, *i.e.* hysteresis.

The isosteric heat of adsorption was determined directly from the adsorption isotherms using the Clausius–Clapeyron equation (Fig. 3, filled squares).[43,44] Also depicted in Fig. 3 is the heat of adsorption calculated according to Van't Hoff (eqn (1)) using the fitted thermodynamic model.[45]

$$\frac{\Delta H_{ads}(X,T)}{RT^2} = -\left(\frac{\partial \ln p}{\partial T}\right)_{X(p,T)} \quad (1)$$

For the largest adsorbed amount, the heat of adsorption ΔH_{ads} remains constant around 2.6 kJ g^{-1}, corresponding to 46.8 kJ mol^{-1}. This value is comparable to those of other Al-based MOFs like aluminium fumarate[9] or CAU-10-H[21] and is only a few percent higher than the heat of vaporization of water.[46] Other ΔH_{ads} reports for MOFs determined mostly higher values.[9,10,13,21,28,43,47] In combination with the water adsorption characteristic, this low value favors the use of MIL-53(Al)-TDC in sorption based chilling, where the released heat of adsorption is tantamount to waste heat.

Multicycle hydrothermal stability and cooling performance

Multicycle stability towards water is a very crucial point when it comes to the envisioned application. Therefore, the sample has been tested in a thermogravimetric setup exposing the sample to a humidified argon flow. Adsorption and desorption are induced by switching the temperature between 40 °C and 140 °C. Prior to and after 20 cycles an equilibrium desorption and adsorption segment was performed. The plot of mass, temperature and water uptake in g g^{-1} over time for 2 × 20 hydrothermal cycles is shown in Fig. 4. Over the first 20 cycles a slight decrease of dry mass (Δm = 1.3%) as well as equilibrium water uptake (ΔX = 3.7%) occurred. This behaviour has been observed before for aluminium fumarate and can be explained by post-synthesis activation of the MOF by the desorbed water comparable to steam distillation.[9] In order to further confirm the stability, a second run of 20 cycles was performed on the same sample. Over these cycles no further decrease in dry mass and just a slight decrease in the equilibrium uptake (ΔX = 2.7%) were observed which is on the order of the balance drift. Conclusively, the material can be suggested to be stable towards cyclic water adsorption and desorption within the test procedure and even more under application related conditions.

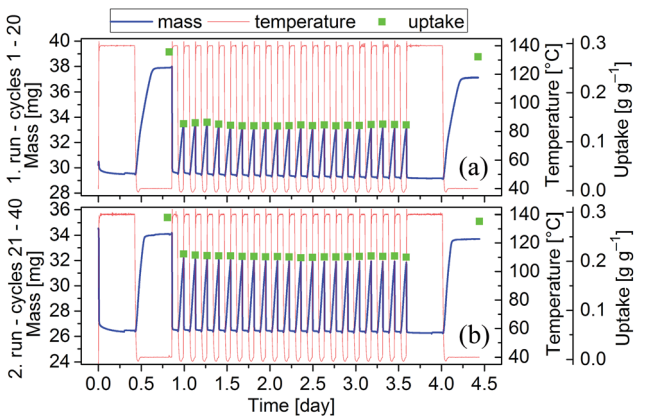

Fig. 4 First (a) and second (b) 20 cycles of adsorption and desorption of MIL-53(Al)-TDC in a thermogravimetric analyzer. Red curve: temperature, blue curve: sample mass, and green dots: uptake.

For additional stability investigations, a fresh sample of the material was investigated with PXRD over 12 cycles at 40 °C with varying humidities. Within the first and the last cycle a complete isotherm ($0 < p/p_0 < 0.8$) was recorded, followed by PXRD (Fig. S1 and S2 in the ESI†), whereas all other cycles only consisted of adsorption at $p/p_0 = 0.8$ and desorption at $p/p_0 = 0.02$.

MIL-53 is known for its breathing effect, that is, a network adapting to guest molecules yielding a wide-pore or narrow pore form.[48] For MIL-53(Al)-TDC we have not observed any reversible or irreversible structural changes upon (repeated) water sorption measurements with *in situ* powder X-ray diffraction. As can be seen from the diffractograms depicted in Fig. 5 (Fig. S2 and S3 in the ESI†), only the height of the peaks reproducibly decreased during adsorption (increasing humidity) and increased during desorption (decreasing humidity). During these cycles no loss in crystallinity and no phase change, which would be marked by additional peaks, can be observed. This result supports MIL-53(Al)-TDC to be structurally stable towards water.

Up to this point, the general suitability of MIL-53(Al)-TDC for adsorption heat transformation has been proven in terms of the demanded S-shaped isotherm, a high maximum water uptake and a good hydrothermal stability. The low heat of adsorption favors MIL-53(Al)-TDC for cooling applications. To further assess the suitability, experimental data were fit using a recently proposed dual-site Langmuir approach,[49,50] which is stated in detail in Section S13 in the ESI.†

During desorption, driving heat (Q_{des}) has to be provided at the adsorbent and heat of condensation (Q_{cond}) has to be discharged at the condenser (*cf.* Fig. 1). The sensitivity of the sample towards these two temperature levels is shown in Fig. 6. As can be seen from this plot, MIL-53(Al)-TDC can almost completely be desorbed at low temperatures between 50 and 70 °C, depending on the condenser temperature. Even at a high condenser temperature of 40 °C a desorption temperature of about 60 °C is sufficient to dry the material, enabling the possibility to dissipate the heat of condensation to the environment *via* heat exchangers. Thus, low temperature waste heat can be utilized that cannot be used for other processes for desorption (see ref. 51 for an overview of waste heat temperature levels).

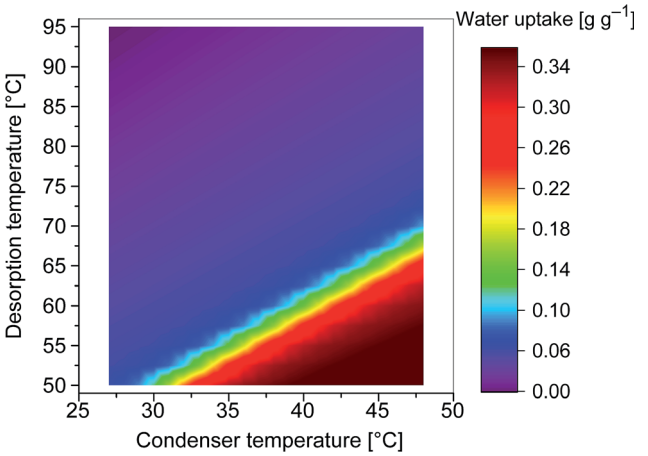

Fig. 6 Sensitivity of uptake capacity towards desorption temperature and condenser temperature, showing that MIL-53(Al)-TDC can be desorbed even at very high condenser temperatures with desorption temperatures below 70 °C.

For the investigation of the adsorption stage, the desorption temperature was fixed at 65 °C, and the water uptake was calculated depending on the evaporation temperature and the heat rejection temperature corresponding to the adsorption temperature (Fig. 7). A desirable high water uptake of 0.35 g g^{-1} can be achieved for comparably high evaporation temperatures of above 15 °C and/or heat rejection below 30 °C. These findings recommend MIL-53(Al)-TDC for thermally driven cooling in industrial processes, as it can work at evaporation temperatures (providing the cooling) above 10 °C on one hand and can be regenerated with waste or solar thermal heat at around 65 °C on the other hand. Thereby, a working window is offered that is not accessible for conventional adsorbents with the corresponding water loading lift.

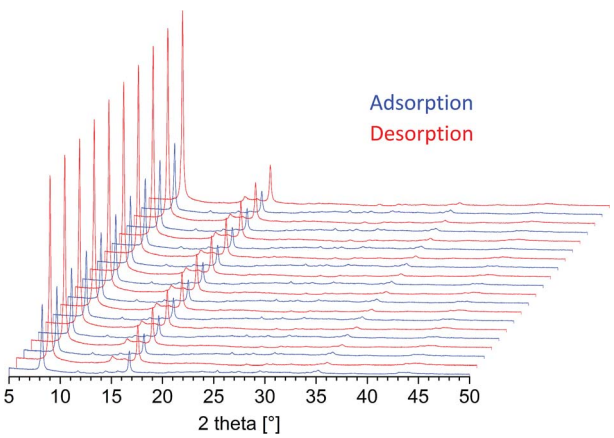

Fig. 5 Ten adsorption (blue)/desorption (red) cycles of MIL-53(Al)-TDC with *in situ* XRD observation, confirming its structural stability upon hydrothermal cycling.

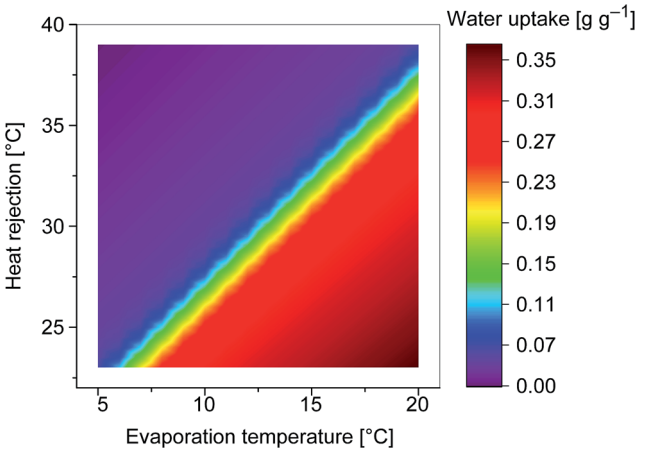

Fig. 7 Water uptake capacity as a function of heat rejection temperature and evaporation temperature, showing a broad plateau for different temperature settings. Drying conditions were set at 65 °C.

Conclusion

MIL-53(Al)-TDC is preferably synthesized from aluminium sulfate or from basic aluminum acetate as water hysteresis is not observed in these cases, which renders this material advantageous for water sorption applications. Extensive water sorption studies followed by *in situ* PXRD and mass balance demonstrated the stability of MIL-53(Al)-TDC during hydrothermal cycling for at least 40 cycles. Besides the technically feasible water uptake of 0.3 g g^{-1}, the low heat of adsorption (2.6 kJ g^{-1}) favors the use of MIL-53(Al)-TDC in chilling processes, since this heat must be rejected to the environment and is waste heat. The thermodynamic evaluation gives good low desorption temperatures at comparably good high condenser temperatures and sufficient water uptake capacities (*cf.* Fig. S17, ESI†) at medium evaporator temperatures. In combination with the previously reported MOFs based on Al^{3+}, like aluminum fumarate or CAU-10-H that show similar stability towards water, the assumption of Al-based MOFs being the most promising MOF adsorbents for application in thermally driven heat transformation can be sustained.

Conflicts of interest

There are no conflicts of interest to declare.

Acknowledgements

The authors gratefully acknowledge the financial support of the Federal German Ministry of Education and Research (BMBF) within the project Optimat under grant no. 03SF0492A/C.

Notes and references

1 H.-C. Zhou, J. R. Long and O. M. Yaghi, *Chem. Rev.*, 2012, **112**, 673–674.
2 M. Eddaoudi, D. B. Moler, H. Li, B. Chen, T. M. Reineke, M. O'Keeffe and O. M. Yaghi, *Acc. Chem. Res.*, 2001, **34**, 319–330.
3 G. Akiyama, R. Matsuda, H. Sato, A. Hori, M. Takata and S. Kitagawa, *Microporous Mesoporous Mater.*, 2012, **157**, 89–93.
4 H. Furukawa, K. E. Cordova, M. O'Keeffe and O. M. Yaghi, *Science*, 2013, **341**, 1230444.
5 N. Stock and S. Biswas, *Chem. Rev.*, 2012, **112**, 933–969.
6 G. Maurin, C. Serre, A. Cooper and G. Férey, *Chem. Soc. Rev.*, 2017, **46**, 3104–3107.
7 M. J. Kalmutzki, C. S. Diercks and O. M. Yaghi, *Adv. Mater.*, 2018, 1704304.
8 F. Fathieh, M. J. Kalmutzki, E. A. Kapustin, P. J. Waller, J. Yang and O. M. Yaghi, *Sci. Adv.*, 2018, **4**, eaat3198.
9 F. Jeremias, D. Fröhlich, C. Janiak and S. K. Henninger, *RSC Adv.*, 2014, **4**, 24073–24082.
10 M. F. de Lange, K. J. F. M. Verouden, T. J. H. Vlugt, J. Gascon and F. Kapteijn, *Chem. Rev.*, 2015, **115**, 12205–12250.
11 J. Canivet, A. Fateeva, Y. Guo, B. Coasne and D. Farrusseng, *Chem. Soc. Rev.*, 2014, **43**, 5594–5617.
12 F. Jeremias, D. Fröhlich, C. Janiak and S. K. Henninger, *New J. Chem.*, 2014, **38**, 1846–1852.
13 F. Jeremias, A. Khutia, S. K. Henninger and C. Janiak, *J. Mater. Chem.*, 2012, **22**, 10148–10151.
14 H. Kummer, F. Jeremias, A. Warlo, G. Füldner, D. Fröhlich, C. Janiak, R. Gläser and S. K. Henninger, *Ind. Eng. Chem. Res.*, 2017, **56**, 8393–8398.
15 D. Lenzen, P. Bendix, H. Reinsch, D. Fröhlich, H. Kummer, M. Möllers, P. P. C. Hügenell, R. Gläser, S. Henninger and N. Stock, *Adv. Mater.*, 2017, **6**, 1705869.
16 M. F. de Lange, T. Zeng, T. J. H. Vlugt, J. Gascon and F. Kapteijn, *CrystEngComm*, 2015, **17**, 5911–5920.
17 A. A. Askalany, M. Salem, I. M. Ismael, A. H. H. Ali, M. G. Morsy and B. B. Saha, *Renewable Sustainable Energy Rev.*, 2013, **19**, 565–572.
18 A. Cadiau, J. S. Lee, D. Damasceno Borges, P. Fabry, T. Devic, M. T. Wharmby, C. Martineau, D. Foucher, F. Taulelle, C.-H. Jun, Y. K. Hwang, N. Stock, M. F. De Lange, F. Kapteijn, G. Gascon, G. Maurin, J.-S. Chang and C. Serre, *Adv. Mater.*, 2015, **27**, 4775–4780.
19 J. Canivet, J. Bonnefoy, C. Daniel, A. Legrand, B. Coasne and D. Farrusseng, *New J. Chem.*, 2014, **38**, 3102–3111.
20 H. Furukawa, F. Gandara, Y.-B. Zhang, J. Jiang, W. L. Queen, M. R. Hudson and O. M. Yaghi, *J. Am. Chem. Soc.*, 2014, **136**, 4369–4381.
21 D. Fröhlich, E. Pantatosaki, P. D. Kolokathis, K. Markey, H. Reinsch, M. Baumgartner, M. A. van der Veen, D. E. de Vos, N. Stock, G. K. Papadopoulos, S. K. Heninnger and C. Janiak, *J. Mater. Chem. A*, 2016, **4**, 11859–11869.
22 S.-I. Kim, T.-U. Yoon, M.-B. Kim, S.-J. Lee, Y. K. Hwang, J.-S. Chang, H.-J. Kim, H.-N. Lee, U.-H. Lee and Y.-S. Bae, *Chem. Eng. J.*, 2016, **286**, 467–475.
23 P. M. Schoenecker, C. G. Carson, H. Jasuja, C. J. J. Flemming and K. S. Walton, *Ind. Eng. Chem. Res.*, 2012, **51**, 6513–6519.
24 S. K. Henninger, G. Munz, K.-F. Ratzsch and P. Schossig, *Renew. Energ.*, 2011, **36**, 3043–3049.
25 A. Khutia, H. U. Rammelberg, T. Schmidt, S. Henninger and C. Janiak, *Chem. Mater.*, 2013, **25**, 790–798.
26 D. Fröhlich, S. K. Henninger and C. Janiak, *Dalton Trans.*, 2014, **43**, 15300–15304.
27 M. F. de Lange, C. P. Ottevanger, M. Wiegman, T. J. H. Vlugt, J. Gascon and F. Kapteijn, *CrystEngComm*, 2015, **17**, 281–285.
28 F. Jeremias, V. Lozan, S. K. Henninger and C. Janiak, *Dalton Trans.*, 2013, **42**, 15967–15973.
29 A. Permyakova, O. Skrylnyk, E. Courbon, M. Affram, S. Wang, U.-H. Lee, A. H. Valekar, F. Nouar, G. Mouchaham, T. Devic, G. D. Weireld, J.-S. Chang, N. Steneou, M. Frère and C. Serre, *ChemSusChem*, 2017, **10**, 1419–1426.
30 N. Ko, P. G. Choi, J. Hong, M. Yeo, S. Sung, K. E. Cordova, H. J. Park, J. K. Yang and J. Kim, *J. Mater. Chem. A*, 2015, **3**, 2057–2064.
31 S. K. Henninger, S.-J. Ernst, L. Gordeeva, P. Bendix, D. Fröhlich, A. D. Grekova, L. Bonaccorsi, Y. Aristov and J. Jaenchen, *Renew. Energ.*, 2017, **110**, 59–68.
32 A. Samokhvalov, *Coord. Chem. Rev.*, 2018, **374**, 236–253.

33 G. Férey, C. Serre, C. Mellot-Draznieks, F. Millange, S. Surblé, J. Dutour and I. Margiolaki, *Angew. Chem.*, 2004, **116**, 6456–6461.
34 C. Volkringer, D. Popov, T. Loiseau, G. Férey, M. Burghammer, C. Riekel, M. Haouas and F. Taulelle, *Chem. Mater.*, 2009, **21**, 5695–5697.
35 E. Alvarez, N. Guillou, C. Martineau, B. Bueken, B. Van de Voorde, C. Le Guillouzer, P. Fabry, F. Nouar, F. Taulelle, D. de Vos, J.-S. Chang, K. H. Cho, N. Ramsahye, T. Devic, M. Daturi, G. Maurin and C. Serre, *Angew. Chem., Int. Ed.*, 2015, **54**, 3664–3668.
36 H. Reinsch, M. A. van der Veen, B. Gil, B. Marszalek, T. Verbiest, D. de Vos and N. Stock, *Chem. Mater.*, 2013, **25**, 17–26.
37 M. H. Bagheri and S. N. Schiffres, *Langmuir*, 2018, **34**, 1908–1915.
38 N. C. Burtch, H. Jasuja and K. S. Walton, *Chem. Rev.*, 2014, **114**, 10575–10612.
39 D. D. Borges, G. Maurin and D. S. Galvão, *MRS Adv.*, 2017, **2**, 519–524.
40 C. W. L. Tschense, N. Reimer, C.-W. Hsu, H. Reinsch, R. Siegel, W.-J. Chen, C.-H. Lin, A. Cadiau, C. Serre, J. Senker and N. Stock, *Z. Anorg. Allg. Chem.*, 2017, **21**, 1600–1608.
41 G. A. González-Martínez, T. Jurado-Vázquez, D. Solís-Ibarra, B. Vargas, E. Sánchez-González, A. Martínez, R. Vargas, E. González-Zamora and I. A. Ibarra, *Dalton Trans.*, 2018, **47**, 9459–9465.
42 M. Thommes, K. Kaneko, A. V. Neimark, J. P. Olivier, F. Rodriguez-Reinoso, J. Roquerol and K. S. W. Sing, *Pure Appl. Chem.*, 2015, **87**, 1051–1069.
43 H. Kim, H. J. Cho, S. Naranayan, S. Yang, H. Furukawa, S. Schiffres, X. Li, Y.-B. Zhang, J. Jiang, O. M. Yaghi and E. N. Wang, *Sci. Rep.*, 2016, **6**, 19097.
44 R. Krishna, *Chem. Eng. Sci.*, 2015, **123**, 191–196.
45 D. M. Ruthven, *Principles of Adsorption and Adsorption Processes*, Wiley, New York, 1984.
46 (*a*) N. S. Osborne, H. F. Stimson and G. C. Ginnings, *J. Res. Natl. Bur. Stand.*, 1939, **23**, 197–260; (*b*) J. A. Dean, *Lange's Handbook of Chemistry*, McGraw-Hill Handbooks, New York, 15th edn, 1998; (*c*) National Institute of Standards and Technology Chemistry WebBook: https://webbook.nist.gov/chemistry/, accessed April 06th, 2018.
47 S. K. Henninger, F. Jeremias, H. Kummer and C. Janiak, *Eur. J. Inorg. Chem.*, 2012, **16**, 2625–2634.
48 C. Serre, F. Millange, C. Thouvenot, M. Noguès, G. Marsolier, D. Louër and G. Férey, *J. Am. Chem. Soc.*, 2002, **124**, 13519–13526.
49 M. Hefti, L. Joss, Z. Bjelobrk and M. Mazzotti, *Faraday Discuss.*, 2016, **192**, 153–179.
50 S.-J. Ernst, M. Baumgartner, D. Fröhlich, H.-J. Bart and S. K. Henninger, *Chem. Ing. Tech.*, 2017, **89**, 1650–1660.
51 S. Brueckner, S. Liu, L. Miró and E. Laevemann, *Appl. Energy*, 2015, **151**, 157–167.

